Microchimica Acta
https://doi.org/10.1007/s00604-019-3472-z

ORIGINAL PAPER

An electrochemical troponin T aptasensor based on the use of a macroporous gold nanostructure

Masoud Negahdary[1,2] · Mostafa Behjati-Ardakani[1] · Hossein Heli[2]

Received: 1 February 2019 / Accepted: 29 April 2019

Abstract

A specific troponin T (TnT) binding aptamer was identified and immobilized on an electrodeposited macroporous gold nanostructure using poly(ethylene glycol) 600, to fabricate a novel and ultrasensitive TnT aptasensor. The transducer surface on the gold disk electrode was characterized by field emission scanning electron microscopy, and immobilization of the aptamer was monitored by open circuit potential measurements. Binding of TnT by the aptamer was monitored by differential pulse voltammetry using ferro/ferricyanide as the redox probe. The aptamer has a high affinity and specificity, and the electrode is sensitive and selective. Best operated at a working potential of 0.23 V (vs. Ag/AgCl), the electrode can detected TnT in the 0.05 to 5.0 ng mL^{-1} concentration range with a 23 pg mL^{-1} detection limit. The method was applied to the determination of TnT in 99 spiked human serum samples, and the diagnostic sensitivity and specificity were 94 and 95%, respectively.

Keywords Biomarker · Biosensor · Aptamer · PEG 600 · Myocardial infarction · Redox marker · Acute coronary syndromes · Myocyte damage · Nanogold · Macropore

Introduction

Troponin is a regulatory protein with three subunits of I (TnI), C and T (TnT) and present in the skeletal and heart muscles [1]. Cardiac troponins of TnT and InI are highly specific for cardiac muscle injury. The cardiac subtype of TnT is specialized for the heart muscle [2]. TnT is used as a sensitive and accurate biomarker to diagnose the acute coronary syndromes and identify myocardial infarction (MI) [3]. In healthy persons, the level of TnT in the bloodstream is negligible or undetectable, but when the heart muscle is damaged, TnT is released and its concentration in the blood increases [3]. In such the conditions, TnI concentration increases too. However, the stability of the released TnT in the blood (ten to fourteen days) is higher than TnI (seven to ten days) [1]. Therefore, TnT is a more sensitive and valuable biomarker than TnI, and early diagnosis of MI by TnT detection is very essential, applicable and important in the fast and effective treatment in the first hours after the occurrence of MI [4]. On the other hand, the Food and Drug Administration recommends TnT measurement as a very useful biomarker in the diagnosis of acute coronary syndromes and the heart failure [5]. A value of TnT level of greater than 0.1 ng mL^{-1} is considered as a damage to the myocardium [5].

The main detection methods of TnT are based on immunoassay. However, there are limitations in these methods, including high cost, complications, interfering effects, and low accuracy. These immunoassays were performed by electrochemical [6], chemiluminescence [7], localized surface plasmon resonance [8], fluorescence and near-infrared fluorescence [9] detections and a field effect transistor [10], in addition to the traditional immunoassay technique [11].

Electronic supplementary material The online version of this article (https://doi.org/10.1007/s00604-019-3472-z) contains supplementary material, which is available to authorized users.

✉ Hossein Heli
hheli7@yahoo.com; heli@sums.ac.ir

[1] Yazd Cardiovascular Research Center, Shahid Sadoughi University of Medical Sciences, Yazd 8916978477, Iran

[2] Nanomedicine and Nanobiology Research Center, Shiraz University of Medical Sciences, Shiraz 71936355899, Iran

Published online: 27 May 2019

Aptamers, as synthetic DNA/RNA sequences, are designed and selected in a way that they have the highest affinity to the target, leading to their applications in drug delivery and discovery, in vitro and in vivo diagnosis, bioimaging, food science, separation techniques, and fabrication of aptamer-based biosensors (aptasensors) [12]. Aptasensors have the advantages of specificity toward analyte due to the in vitro procedure of aptamer selection (systematic evolution of ligands by exponential enrichment, SELEX), developable for a variety of analytes (some other recognition elements such as antibodies are not available for any analyte), inertness, tenability in the sequence design and chemical modifications, stability and long shelf life. As for the aptasensing, different transduction routes such as electrochemical [12], photoelectrochemical [13], optical [14] and mass [15] have been introduced. Electrochemical aptasensing have the advantages of high sensitivity, low cost, simplicity, fast response detection, with using lower amounts of aptamers without using labeling. Aptasensors have been proposed for detecting different biomarkers [12], including those for the detection of MI [16].

In nanotechnology, increase in surface to volume ratio, incidence of quantum confident effect, enhancement in chemical reactivity and appearance of different physicochemical properties of nanomaterials (compared to large scale ones) have led to applications of nanostructured materials in fabrication of (electro)chemical sensors and biosensors [17–19]. In addition, accuracy and specificity of the biosensors can be improved using nanostructured transducers [17–19]. Gold nanostructures have a high stability, accessibility, lack of toxicity and biocompatibility with huge biomedical (including biosensing) applications [12, 17].

In the present study, a TnT specific 40-mer aptamer was immobilized on the surface of a macroporous gold nanostructure, and a novel TnT aptasensor was presented. This TnT electrochemical aptasensor provided a new achievement in the early detection of MI.

Materials and methods

Materials and biologicals

Materials and reagents were purchased from Sigma (USA, sigmaaldrich.com), Merck (Germany, merckgroup.com) or Scharlau (Spain, scharlab.com) without further purification. Cardiac TnT, human serum albumin (HSA), bilirubin, heparin sodium salt and hemoglobin were purchased from Sigma (USA, sigmaaldrich.com). Deionized water was used throughout the work. A specific 40-mer thiolated aptamer [20] was prepared from Bioneer Co. (Korea, bioneer.com) with the sequence of:

5′-(SH)-$(CH_2)_6$-CGTGCAGTACGCCAACCTTT CTCATGCGCTGCCCCTCTTA-3′.

Apparatus

Surface morphology of the macroporous gold nanostructure was evaluated by field emission scanning electron microscopy (FESEM), using a TESCAN Mira 3-XMU (Czech Republic, www.tescan.com) equipped with energy-dispersive X-ray spectroscopy (EDS). All electrochemical measurements were performed by a potentiostat/galvanostat of μ-Autolab (the Netherlands, www.metrohm-autolab.com) run through GPES software. Differential pulse voltammetry (DPV) technique was used for the quantitation of TnT with a pulse width of 25 mV, a pulse time of 50 ms, and a scan rate of 10 mV s^{-1}. A gold disk (Au) of 2 mm diameter from Azar Electrode Co. (Iran, www.azarelectrode.ir), an Ag/AgCl, 3 mol L^{-1} KCl and a platinum disk from Azar Electrode Co. (Iran, www.azarelectrode.ir) were employed as the working, reference and counter electrodes, respectively. In order to find an optimized time for immobilization of the aptamer on the surface of macroporous gold nanostructure, screen printed gold electrodes from DropSens (Spain, www.dropsens.com) were employed, macroporous gold nanostructure was electrodeposited on their working surfaces, and open circuit potential (OCP) was measured in a two-electrode configuration using a digital multimeter of Mastech MS8340B (China, www.mastech-group.com).

Preparation of the gold electrode covered with macroporous gold nanostructure (Au/MGN electrode)

Macroporous gold nanostructure was electrodeposited for the first time. A gold electrode was firstly polished by sand polishing and then 50 nm-alumina powder; when the electrode surface was like a mirror, it was inserted in a tube containing an ethanol/water (3:1) mixture and ultrasonicated in an ultrasound bath during 6 min. At the next step, the electrode was immersed in a cell containing 5 mL H_2SO_4 (0.5 mol L^{-1}) containing $HAuCl_4$ (20 mmol L^{-1}) and poly(ethylene glycol) (PEG) 600 (0.1 mol L^{-1}). Macroporous gold nanostructure was electrodeposited at 0 mV for 5 min. The Au/MGN electrode was store at ambient temperature in the lab.

Immobilization of the aptamer on the Au/MGN electrode surface

Before any immobilization, inter-thiol-thiol bonds were broken by adding 10 μL dithiothreitol (DTT) solution (500 mmol L^{-1}) containing 10 mmol L^{-1} sodium acetate at pH 5.2. The mixture was mixed for 20 min at room temperature, and then ethyl acetate was added three times (total volume of 100 μL); after each addition, the upper layer was discarded. Then, 10 mmol L^{-1} phosphate buffer solution containing 5.0 mmol L^{-1} NaCl, 2.0 mmol L^{-1} KCl and 1.0 mmol L^{-1} $MgCl_2$ at pH 7.4 was added to attain a 10 μmol L^{-1} aptamer solution. 10 μL of the aptamer solution was dropped on the surface of the Au/MGN electrode. The electrode was refrigerated at 4 °C to complete immobilization process for an optimized time of 60 min. The electrode was then rinsed with deionized water and then 10 μL of mercaptohexanol (MCH, 1.0 mmol L^{-1}) was drooped on the electrode and kept at room temperature for 30 min. MCH was used to block the unimmobilized sites on the surface and alignment of the aptamer monolayer. The electrode (the aptasensor) was rinsed with deionized water and when it was not used, it was kept refrigerated in Tris-HCl buffer (20 mmol L^{-1}).

Nyquist diagrams were recorded using both the Au/MGN electrode and the aptasensor in a solution of Tris-HCl buffer (20 mmol L^{-1}) containing KCl (0.5 mol L^{-1}) and ferro/ferricyanide redox marker (0.5 mol L^{-1}). The dc-offset potential was equal to the equilibrium potential of the system (equal to 210 mV vs. Ag/AgCl), the frequency range was 100 kHz to 25 mHz, the ac voltage amplitude was 10 mV and the equilibrium time was 5 s. The system was run on a PC using FRA 4.9 software.

Aptasensor targeting with TnT

Binding process of TnT (with various concentrations) with the immobilized aptamers was followed at 37 °C. The optimized binding time was achieved as 31 min and this time was used in all binding processes between aptamer and TnT. After this binding time, the electrode was rinsed with deionized water and immersed in a solution of Tris-HCl buffer (20 mmol L^{-1}) containing KCl (0.5 mol L^{-1}) and ferro/ferricyanide redox marker (0.5 mol L^{-1}), and DPV plots were separately recorded after binding each concentration of TnT for the oxidation of the redox marker.

Real samples analyses

Real samples were obtained from 99 human's blood serum (50 women and 49 men) and classified in four groups of 48 MI patients, 41 healthy persons, 5 with kidney disease, and 5 with liver disease (the last two groups were selected to find actual performance of the aptasensor and prevent false positive results of TnT in patients). Before any sampling, the informed consent was signed by the persons, and all of the procedures were followed according to the guidelines of the Ethics Committee of the Shiraz University of Medical Sciences (license number 14588). The MI patients were previously identified by determination of TnI levels, using an AccuBind® ELISA Kit from Monobind Inc. (USA, www.monobind.com). It is also known that TnT level necessarily increases along with TnI in MI patients [21]. False positive result was a result obtained by the aptasensor indicating a person to be patient, while it was not, and false negative one was a result obtained by the aptasensor indicating a person to be healthy, while it was patient.

Results and discussion

Morphology of the gold (Au and Au/MGN electrodes) surfaces was investigated by FESEM (Fig. 1a-f), and an EDS from the gold nanostructure (Fig. 1g) was recorded. FESEM images reveal that while the gold electrode has a relatively smooth surface, the surface of the electrodeposited gold nanostructure is rough. The low-magnified images of the gold nanostructure show a highly porous structure entirely covering the surface similar to ensembles, and each ensemble itself comprises of macroporous regular dripstone-like of gold with thin edges of 22 ± 8 nm. This special morphology can provide a high surface area and roughness factor for hosting of the immobilized aptamer. The EDS spectrum also indicates that the gold nanostructure is highly pure. Electrochemically attainable surfaces of the gold substrate and macroporous gold nanostructure were determined by recording cyclic voltammograms at different potential sweep rates in a solution of Tris-HCl buffer (20 mmol L^{-1}) containing KCl (0.5 mol L^{-1}) and ferro/ferricyanide redox marker (0.5 mol L^{-1}), using the gold and Au/MGN electrodes (data not shown). Based on a classical analysis of the peak currents of the voltammograms, Randles-Sevcik equation, and the diffusion coefficient of the redox marker, the real surface areas of the electrodes accessible for the aptamer to be immobilized are found as 0.035 and 0.20 cm^2 for Au and Au/MGN electrodes, respectively. This indicates a roughness factor of 5.7 for the gold nanostructure.

It has been reported that $AuCl_4^-$ forms complex with PEG-polypropylene glycol-PEG block copolymers [22, 23] by formation of pseudo crown ether structures those are induced by ion-dipole interactions [22–24]. Therefore, PEG 600 binds to the gold ionic species. Although a high negative overpotential was applied for the electrodeposition of the macroporous gold nanostructure (vs. AgCl, 0 V, compared to 1.27 V for the standard redox potential of Au^{3+}/Au redox couple), due to binding of the gold species to PEG 600, there was a negative shift in the thermodynamic potential of the Au^{3+}/Au redox

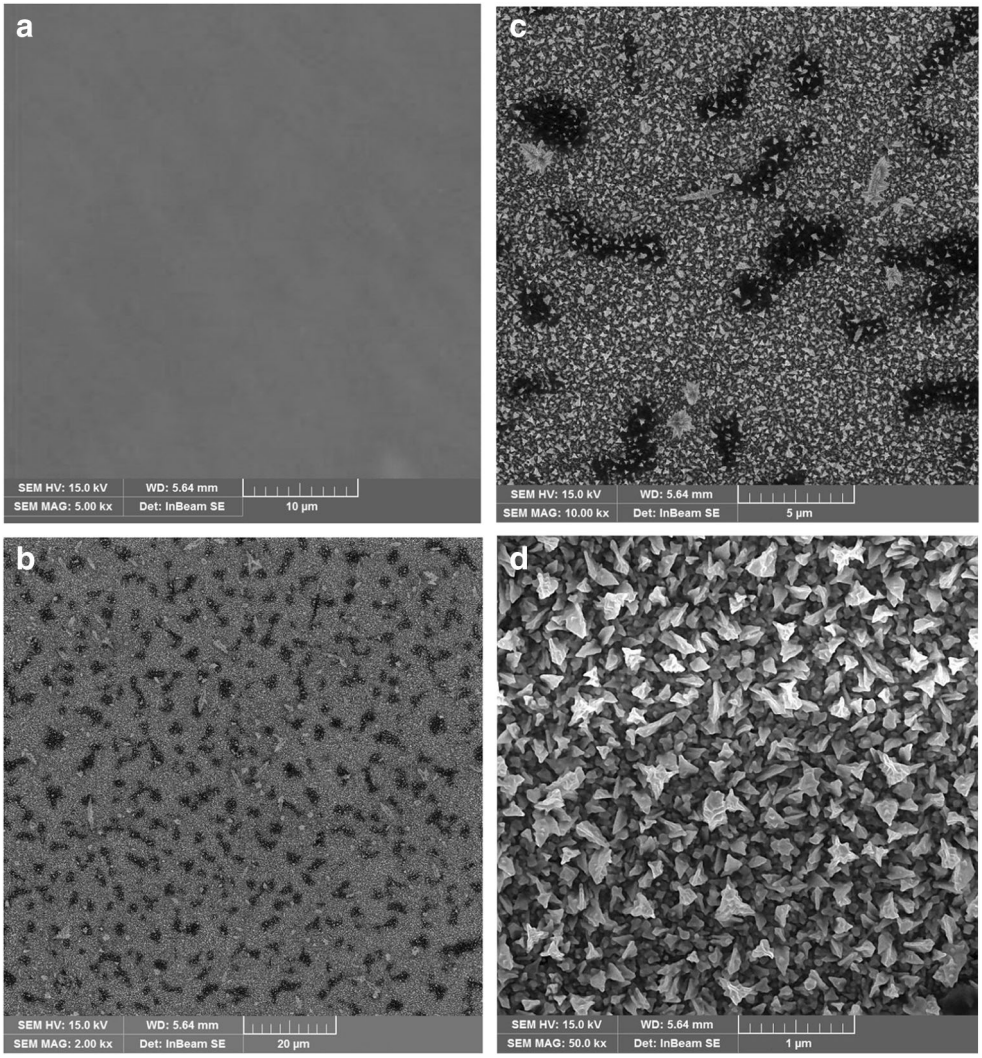

Fig. 1 A FESEM image from the gold electrode surface (**a**), FESEM images from the macroporous gold nanostructure at different magnifications (**b**-**f**), and a EDS from the macroporous gold nanostructure (**g**)

couple. Hence, formation of the preliminary gold nuclei occurred under the control of charge transfer kinetics. PEG 600 can also play, on the other hand, the role of a shape-directing agent and control the directions of nucleation and growth, leading to an anisotropic structure. Formation of different shapes of gold nanostructures in the presence of diols [25], and amino acids [26] has also been reported elsewhere.

In order to electrochemical characterization of the gold electrodes employed in this study, cyclic voltammograms of gold, Au/MGN, the aptasensor and the aptasensor after targeting with TnT in the presence of the redox marker were recorded, while the optimized experimental conditions applied throughout the study (vide infra) were followed. The results are presented in Fig. 2. Based on the results, the Au/MGN electrode represents larger peak currents related to increment in the real surface area of this electrode, compared to the gold electrode. Upon immobilization of the aptamer on the Au/MGN electrode surface, the peak currents of the redox marker decrease with a bit change in the formal (as the mid peak) potential. These are due to change in the entity of the electrode surface after aptamer immobilization; the redox marker should approach to a surface covered by a self-assembled monolayer of the aptamer. The aptamer contains a net negative charge due to its phosphate-sugar backbone, and the redox marker has a certain access to the aptasensor surface. This access is certainly limited, compared to the Au/MGN electrode surface due to the negative charge of the aptamer. Targeting the aptasensor with TnT causes to further decrement in the peak current due to repelling the redox marker from the aptamer-TnT complex. TnT has an isoelectric point of 4.98 to 5.9 [27], and its binding to the aptamer leads to an increment in the negative surface charge. Therefore, upon binding TnT, fewer redox markers can be attained to approach the surface (repels from the aptasensor surface), and the peak currents lower. The fabrication and working principles of the aptasensor are summarized in Scheme 1.

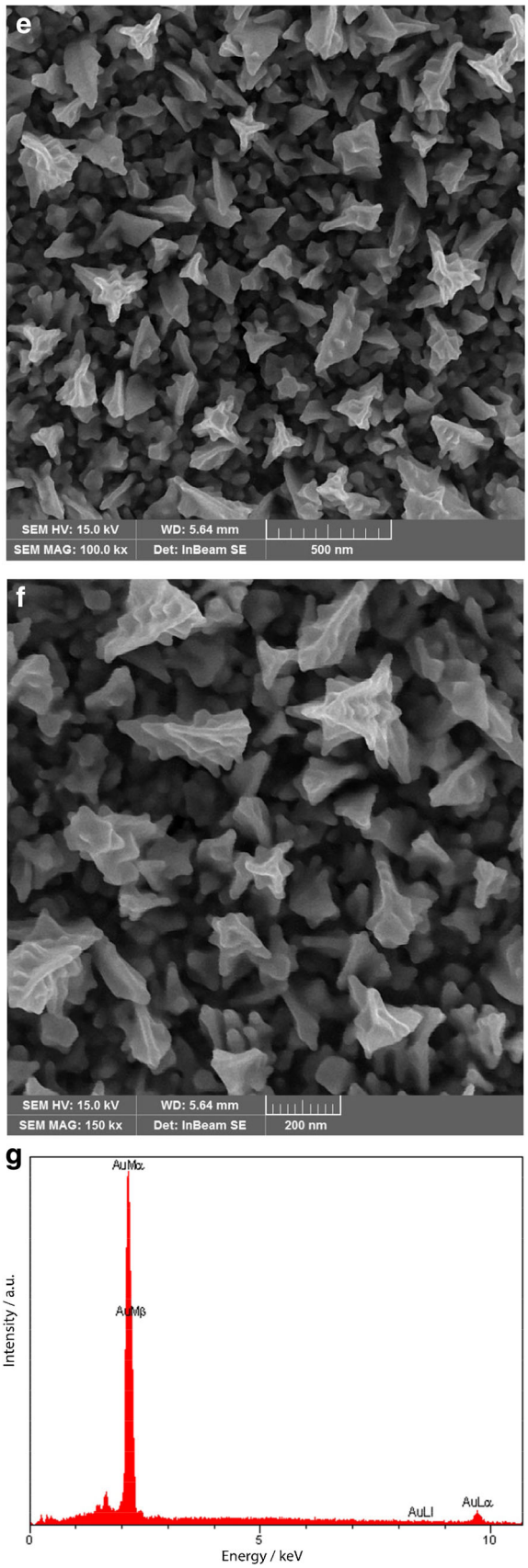

Fig. 1 (continued)

In order to optimize the time of immobilization of the aptamer on the Au/MGN electrode surface, a droplet of the aptamer solution of 10 μmol L^{-1} was placed on the electrode surface, and OCP was measured for the duration of 1.5 h. The data is shown in supplementary material S1 as OCP variation with time. When a negatively charged species such as the aptamer is immobilized on a surface, its accumulation on the surface changes the electrode potential recordable by measuring OCP, and reaching to a stable OCP indicates that immobilization of the species on the surface to be completed. It should also be added that because a two-electrode configuration was employed to measure OCP, the sign of potential is meaningless. In supplementary material S1, OCP continuously changes from the initial time of aptamer immobilization and reaches a constant value during 60 min. Therefore, 60 min is selected as the optimized time of aptamer immobilization.

Supplementary material S2 shows Nyquist diagrams recorded using the Au/MGN electrode and the aptasensor. Electrical equivalent circuits compatible with theses Nyquist diagrams are presented in supplementary material S3. The values of the circuit elements were obtained by fitting the diagrams on the circuits, and are presented in supplementary material S4. Based on these values, and by comparing the high-frequency responses of the Au/MGN electrode and the aptasensor, it is revealed that aptamer immobilization on the Au/MGN electrode surface does not markedly affect the conductivity of the substrate, because the ohmic series resistance remains almost unchanged upon aptamer immobilization on the Au/MGN electrode surface.

To find an optimized binding time of TnT to the aptasensor, we firstly recorded a DPV by the aptasensor as explained in section 2.5; then, a 1.0 ng mL^{-1} concentration of TnT was bound to the aptasensor and incubated at 37 °C; DPVs were recorded at incubation time intervals of 5 min and the data is presented in supplementary material S5. The peak current in DPVs decreases upon increment in the incubation (binding) time, and reaches a steady value after 31 min. This time is, therefore, selected as the optimal time of the aptasensor targeting with TnT.

Figure 3 shows DPVs recorded for the aptasensor after targeting with TnT of different concentrations at the optimized experimental conditions of the aptasensor-TnT binding. Upon increment in the TnT concentration, the peak current in DPVs decreases. Upon increment in the amount of bound TnT, the negative surface charge of the aptasensor increases due to the negative charge of TnT, and the peak current lowers. The peak current in DPVs depends on the TnT concentration in a range from 0.05 to 5.0 ng mL^{-1}. The respective calibration plot is shown in the inset of Fig. 3. The calibration plot has a regression equation of $I_p = (-2.22 \pm 0.07)\ \log C_{TnT} + (1.66 \pm 0.05)$. Limit of detection (LOD) of the aptasensor for the detection of TnT is obtained using a signal equal to S-3 × SD, where S and SD are the average and the standard deviation of the

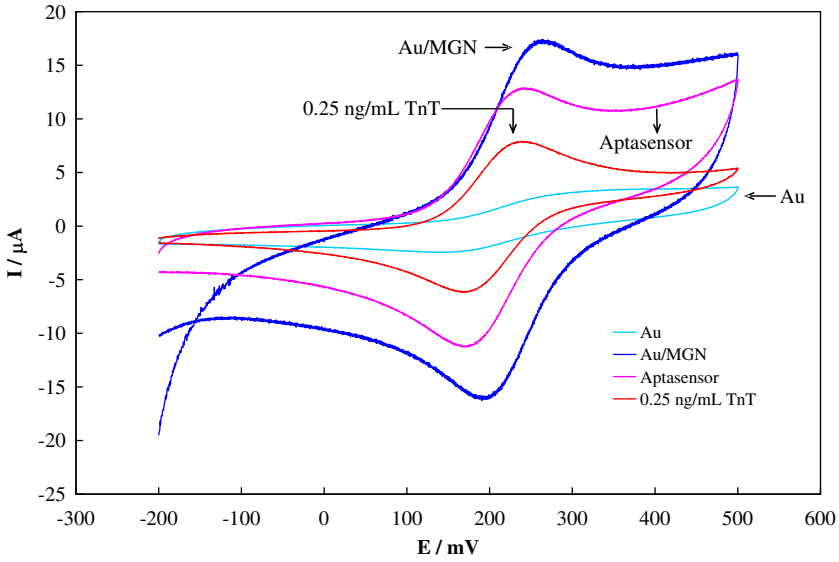

Fig. 2 Cyclic voltammograms of gold, Au/MGN, the aptasensor and the aptasensor after targeting with 0.25 ng mL^{-1} TnT recorded for the redox marker. For the preparation of the aptasensor, the optimized experimental conditions were applied. The potential sweep rate was 50 mV s^{-1}

aptasensor signal in the absence of TnT, respectively. This value is obtained as LOD = 23 pg mL^{-1}. In Table 1, some of the different TnT sensing methods are summarized. Based on this comparison, the present study is the unique aptasensor

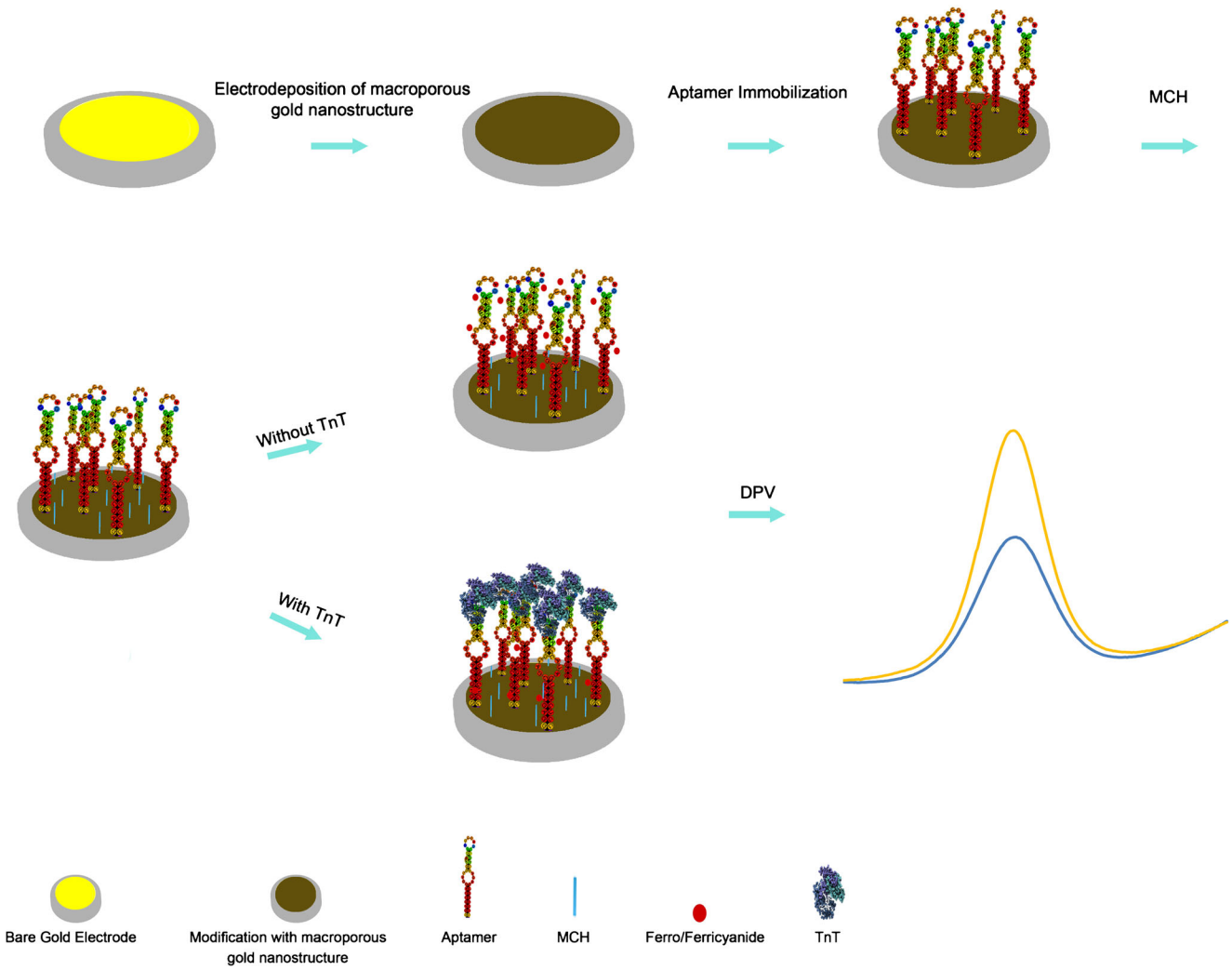

Scheme 1 The fabrication and working principles of the aptasensor

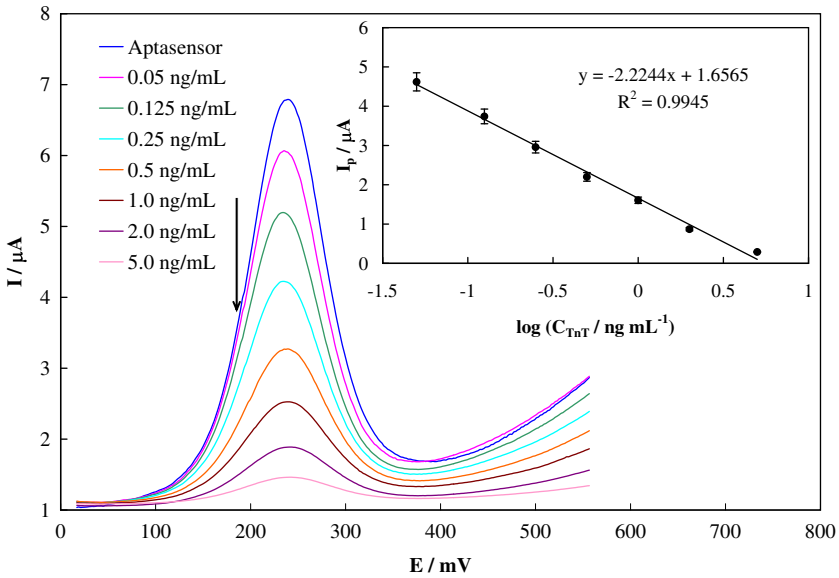

Fig. 3 DPVs of the aptasensor before and after binding with different concentrations of TnT. Inset: A calibration plot for the dependency of the peak currents in the main panel on the TnT concentration (the error bars refer to five times replicates)

reported for the detection of TnT. The aptasensor represented a comparable dynamic range and a better or comparable LOD, and is applicable for analysis of serum samples. The majority of the other reported methods for sensing TnT was based on immunosensing. However, in aptasensors, aptamers (as a sensing element) have some advantages such as high affinity and specificity to capture the analyte due to their 3D sequence-dependent structures, low immunogenicity and toxicity, lower cost, and higher reproducibility and thermal stability, compared to antibodies in immunosensors.

In order to inspect the repeatability and reproducibility of the aptasensor, TnT of two levels were determined through independent measurements over a same day (intra-day assay) and different days (inter-day assay), and the results are presented in supplementary material S6. Moreover, 0.5 ng mL^{-1} of TnT was quantified three times using one aptasensor and a relative standard deviation (RSD) of 2.4% was obtained.

The reproducibility of fabrication of the aptasensor was investigated after 6 times of fabrication. The aptasensor was prepared, bound with TnT, and the related DPVs were recorded. Then, the aptasensor was washed with the piranha solution, fabricated again and DPVs were recorded. The data are presented in supplementary material S7. RSD was found for the aptasensor signals during this procedure as 2.6%. Therefore, the aptasensor has excellent fabrication reproducibility.

In order to perform the regeneration ability of the aptasensor, it was bound with 0.5 ng mL^{-1} concentration of TnT and DPVs were recorded before and after binding. Then, the aptasensor was immersed in deionized water of 95 °C for 5 min to break the bonds between the aptamer and TnT, and then re-bound with the same concentration of TnT. This cycle was repeated 7 times in a similar fashion. The difference in values between the peak currents in DPVs, before and after binding, was found to have a RSD value of 5.1%. Therefore, the aptasensor is reusable after each sample analysis by dipping in hot water, and then it will be usable for analysis of another sample.

As to exploration of the stability of the aptasensor, it was bound with a 0.5 ng mL^{-1} concentration of TnT, and DPVs were recorded for consecutive days, while it was placed in Tris-HCl buffer (20 mmol L^{-1}) at 4 °C for storage during this time. The results are shown in supplementary material S8. Based on the results, the aptasensor signal kept its 90% of the initial value after 9 days, and this time is considered as the stability time of the aptasensor.

In order to evaluate the selectivity of the designed TnT aptasensor, several interfering agents including bilirubin, ethylenediaminetetraacetic acid (EDTA), hemoglobin, heparin and HSA were tested with four concentrations of 0.5, 5, 20 and 50 ng mL^{-1}. The results for this experiment are shown in supplementary material S9. The aptasensor did not show a significant response against these interferences at all of the evaluated concentrations and it is considered selective.

To judge the applicability performance of the aptasensor, human blood seras from 99 individuals were analyzed. These samples were classified into four groups of healthy persons (41 members), MI patients (48 members), kidney disease patients (5 members) and liver disease patients (5 members). The samples of MI were detected in a hospital by analysis of TnI levels, using a method of immunoassay. The threshold level of TnT in a serum sample to decide a person to be a MI patient is 0.1 ng mL^{-1} [5]. On the other hand, the limit of quantitation of a detection method is defined as a concentration producing a signal equal to 10 × SD [58], and since the aptasensor is a signal-off type with a logarithmic concentration dependent of the signal, we assumed a signal produced by a sample ≤ S_T-10 × SD to be considered a MI patient (positive), where S_T is the aptasensor signal for the MI threshold level of TnT. The results for the analyses of human blood serums are summarized in supplementary material S10,

Table 1 Comparison of different TnT sensing methods

Detection method	Nanomaterial employed	Sample	Detection range	LOD	Ref.
Immunosensing	–	Serum	0.5–25 μg L^{-1}	–	[28]
Immunosensing	–	Whole blood	–	–	[11]
Immunosensing	–	Serum	0.1–15 μg L^{-1}	–	[29]
Immunosensing	–	Plasma	0.01–0.029 μg L^{-1}	0.01 ng mL^{-1}	[30]
Immunosensing	–	Fasting blood, urine	0.003–0.014 ng mL^{-1}	3 pg mL^{-1}	[31]
Immunosensing	Au nanoparticles	Serum	<0.15 nmol L^{-1}	0.02 nmol L^{-1}	[32]
Immunosensing	–	Plasma	>0.0133 μg L^{-1}	1 ng L^{-1}	[33]
Immunosensing	–	Serum	>0.014 μg	2 ng L^{-1}	[34]
Electrochemical immunosensing	Carbon nanotubes	Serum	0.02–0.32 ng mL^{-1}	16 pg mL^{-1}	[6]
Electrochemical immunosensing	–	Serum	0.025–4.0 ng mL^{-1}	8 pg mL^{-1}	[35]
Electrochemical immunosensing	Carbon nanotubes	Serum	0.0025–0.5 ng mL^{-1}	3.5 pg mL^{-1}	[36]
Electrochemical immunosensing	–	Serum	0.05–1 ng mL^{-1}	17 pg mL^{-1}	[37]
Electrochemical immunosensing	Graphite nanoplatelets/Au nanoparticles	Plasma	0.05–0.35 ng mL^{-1}	16 pg mL^{-1}	[38]
Electrochemical immunosensing	–	Plasma	–	8.8 pg L^{-1}	[39]
Electrochemical immunosensing	Au nanoparticles	Serum	0.20–1.00 ng mL^{-1}	100 pg mL^{-1}	[40]
Electrochemical immunosensing	Carbon nanotubes	Serum	0.1 and 10 ng mL^{-1}	33 pg mL^{-1}	[41]
Electrochemical immunosensing	SiO_2 nanostructure	–	100 pg mL^{-1}-1 mg mL^{-1}	100 pg mL^{-1}	[42]
Electrochemical immunosensing	Au nanoparticles	Serum	0.00001–100 pg mL^{-1}	–	[43]
Electrochemical immunosensing	–	Serum	0.05–5.0 ng mL^{-1}	16 pgmL^{-1}	[44]
Electrochemical immunosensing	Nanotextured ZnO	Serum	10 fg mL^{-1}-1 ng mL^{-1}	10 fg mL^{-1}	[45]
Electrochemical immunosensing	–	Serum	0.1–10 ng mL^{-1}	0.2 ng mL^{-1}	[46]
Electrochemical immunosensing	Au nanoparticles	Serum, plasma	0.1–0.9 ng mL^{-1}	76 pg mL^{-1}	[47]
Surface plasmon resonance immunosensing	–	Serum	0.03–6.5 ngmL^{-1}	10 pg mL^{-1}	[8]
Surface plasmon resonance immunosensing	–	Serum	0.5–40 ng mL^{-1}	5 ng mL^{-1}	[48]
Surface plasmon resonance immunosensing	–	Serum	0.05–4.5 ng mL^{-1}	–	[49]
Surface plasmon resonance immunosensing	–	–	< 50 μg mL^{-1}	100 ng mL^{-1}	[50]
Localized surface plasmon resonance immunosensing	Au nanorods	–	7.6×10^{-15}-9.1×10^{-4} g mL^{-1}	0.5 ng mL^{-1}	[51]
Localized surface plasmon resonance immunosensing	Nanoporous alumina	–	>1 pg mL^{-1}	1 ng mL^{-1}	[52]
Fluorescence immunosensing	–	Plasma	0.5–40 nmol L^{-1}	0.5 nmol L^{-1}	[9]
NIR fluorescent immunosensing	Carbon nanotubes	Serum, whole blood	–	100 ng mL^{-1}	[53]
Electrical immunosensing	Carbon nanotubes	Serum	–	0.16 μg mL^{-1}	[54]
Electrical immunosensing	–	Plasma	10 ng mL^{-1}-100 fg mL^{-1}	1 pg mL^{-1}	[55]
Electrical sensing	Si nanowires	Whole blood	> 1 nmol L^{-1}	–	[10]
Electrical sensing	Si nanowires	Serum	>1 fg mL^{-1}	–	[56]
Electrochemical aptasensing	Pt wire	–	0.005–0.04 ng mL^{-1}	–	[57]
Electrochemical aptasensing	Macroporous Au nanostructure	Serum	0.05–5 ng mL^{-1}	23 pg mL^{-1}	This work

indicating two false positive with three false negative results. Therefore, diagnostic sensitivity of the aptasensor is 94% and its diagnostic specificity is 95%.

Conclusion

Selection of a specific aptamer accompanied with applying nanotechnology in the design of an aptasensor for biomarkers has led to the improvement in sensitivity and selectivity with high accuracy detections. Upon damage to cardiac myocytes, TnT is released to the bloodstream, and as a specific biomarker, it can be detected by the aptasensor. High stability, regeneration and reproducibility of this aptasensor can introduce a new method in clinical diagnosis of MI, especially in the early stages for a quick start of treatment. The method of synthesis of gold nanostructure can also be expanded to fabrication of diverse nanostructures to attain higher surface concentration of immobilized biorecognition elements. The aptasensor can also be fabricated by another aptamer to improve the figure of merits.

Acknowledgments We would like to thank the Research Councils of Shiraz University of Medical Sciences (14588) and Shahid Sadoughi University of Medical Sciences for supporting this research.

Compliance with ethical standards The author(s) declare that they have no competing interests.

References

1. Mair J, Thygesen K (2016) Using cardiac troponins in patients with acute myocardial infarction. In: Maisel AS, Jaffe AS (eds) Cardiac biomarkers: case studies and clinical correlations. Springer International Publishing, Cham, pp 57–68. https://doi.org/10.1007/978-3-319-42982-3_5
2. Seliger SL, Hong SN, Christenson RH, Kronmal R, Daniels LB, Lima JA, de Lemos JA, Bertoni A (2017) High-sensitive cardiac troponin T as an early biochemical signature for clinical and subclinical heart failure. Circulation 135(16):1494–1505
3. Mueller C, Giannitsis E, Christ M, Ordóñez-Llanos J, McCord J, Body R, Panteghini M, Jernberg T, Plebani M, Verschuren F (2016) Multicenter evaluation of a 0-hour/1-hour algorithm in the diagnosis of myocardial infarction with high-sensitivity cardiac troponin T. Ann Emerg Med 68(1):76–87 e74
4. Ascef B, Izidoro J, Almeida A, Neto AB, Júnior AG, Acurcio F (2016) Effectiveness and safety of thrombolytic agents streptokinase, Alteplase and Tenecteplase in the treatment of acute myocardial infarction. Value Health 19(7):A640
5. Ohman EM, Armstrong PW, Christenson RH, Granger CB, Katus HA, Hamm CW, O'Hanesian MA, Wagner GS, Kleiman NS, Harrell FE Jr, Califf RM, Topol EJ (1996) Cardiac troponin T levels for risk stratification in acute myocardial ischemia. GUSTO IIA investigators. N Engl J Med 335(18):1333–1341. https://doi.org/10.1056/nejm199610313351801
6. Freitas TA, Mattos AB, Silva BV, Dutra RF (2014) Amino-functionalization of carbon nanotubes by using a factorial design: human cardiac troponin T immunosensing application. Biomed Res Int 2014
7. Zong C, Zhang D, Yang H, Wang S, Chu M, Li P (2017) Chemiluminescence immunoassay for cardiac troponin T by using silver nanoparticles functionalized with hemin/G-quadruplex DNAzyme on a glass chip array. Microchim Acta:1–8
8. Dutra RF, Kubota LT (2007) An SPR immunosensor for human cardiac troponin T using specific binding avidin to biotin at carboxymethyldextran-modified gold chip. Clin Chim Acta 376(1):114–120
9. Qiao Y, Tang H, Munske GR, Dutta P, Ivory CF, Dong W-J (2011) Enhanced fluorescence anisotropy assay for human cardiac troponin I and T detection. J Fluoresc 21(6):2101–2110
10. Livi P, Kwiat M, Shadmani A, Pevzner A, Navarra G, Jr R, Stettler A, Chen Y, Patolsky F, Hierlemann A (2015) Monolithic integration of a silicon nanowire field-effect transistors array on a complementary metal-oxide semiconductor chip for biochemical sensor applications. Anal Chem 87(19):9982–9990
11. Hamm CW, Goldmann BU, Heeschen C, Kreymann G, Berger J, Meinertz T (1997) Emergency room triage of patients with acute chest pain by means of rapid testing for cardiac troponin T or troponin I. N Engl J Med 337(23):1648–1653. https://doi.org/10.1056/nejm199712043372302
12. Rahi A, Sattarahmady N, Heli H (2016) Label-free electrochemical aptasensing of the human prostate-specific antigen using gold nanospears. Talanta 156:218–224
13. Zhao W-W, Xu J-J, Chen H-Y (2016) Photoelectrochemical aptasensing. TrAC Trends Anal Chem 82:307–315
14. Ng S, Lim HS, Ma Q, Gao Z (2016) Optical aptasensors for adenosine triphosphate. Theranostics 6(10):1683
15. Dong Z-M, Zhao G-C (2012) Quartz crystal microbalance aptasensor for sensitive detection of mercury(ii) based on signal amplification with gold nanoparticles. Sensors (Basel) 12:7080–7094
16. Bini A, Centi S, Tombelli S, Minunni M, Mascini M (2008) Development of an optical RNA-based aptasensor for C-reactive protein. Anal Bioanal Chem 390(4):1077–1086
17. Tondro GH, Dehdari Vais R, Sattarahmady N (2018) An optical genosensor for enterococcus faecalis using conjugated goldnanoparticles-rRNA oligonucleotide. Sensors Actuators B Chem 263:36–42
18. Sattarahmady N, Heli H, Vais RD (2014) A flower-like nickel oxide nanostructure: synthesis and application for choline sensing. Talanta 119:207–213
19. Heli H, Majdi S, Jabbari A, Sattarahmady N, Moosavi-Movahedi A (2010) Electrooxidation of dextromethorphan on a carbon nanotube–carbon microparticle–ionic liquid composite: applied to determination in pharmaceutical forms. J Solid State Electrochem 14(8):1515–1523
20. Ban C, Song K-M, Jeong W (2012) United States patent application publication, pub. No.: US 2012/0316326 A1
21. Morrow DA (2010) Cardiovascular biomarkers: pathophysiology and disease management. Springer Science & Business Media
22. Sakai T, Alexandridis P (2004) Single-step synthesis and stabilization of metal nanoparticles in aqueous Pluronic block copolymer solutions at ambient temperature. Langmuir 20(20):8426–8430
23. Sakai T, Alexandridis P (2005) Mechanism of metal ion reduction, nanoparticle growth and size control in aqueous amphiphilic block copolymer solutions at ambient conditions. J Phys Chem B 109(16):7766–7777
24. Longenberger L, Mills G (1995) Formation of metal particles in aqueous solutions by reactions of metal complexes with polymers. J Phys Chem 99(2):475–478
25. Bi Y, Lu G (2008) Morphological controlled synthesis and catalytic activities of gold nanocrystals. Mater Lett 62(17):2696–2699
26. Vais RD, Sattarahmady N, Karimian K, Heli H (2015) Green electrodeposition of gold hierarchical dendrites of pyramidal

nanoparticles and determination of azathioprine. Sensors Actuators B Chem 215:113–118
27. Iwańska E, Mikołajczak B, Grześ B, Pospiech E (2016) Impact of post mortem aging of pork on changes in the isoelectric point of the proteins and tenderness. Med Weter 72(7):458–462
28. Katus HA, Remppis A, Neumann FJ, Scheffold T, Diederich KW, Vinar G, Noe A, Matern G, Kuebler W (1991) Diagnostic efficiency of troponin T measurements in acute myocardial infarction. Circulation 83(3):902–912
29. Katus HA, Looser S, Hallermayer K, Remppis A, Scheffold T, Borgya A, Essig U, Geuss U (1992) Development and in vitro characterization of a new immunoassay of cardiac troponin T. Clin Chem 38(3):386–393
30. Wallace TW, Abdullah SM, Drazner MH, Das SR, Khera A, McGuire DK, Wians F, Sabatine MS, Morrow DA, de Lemos JA (2006) Prevalence and determinants of troponin T elevation in the general population. Circulation 113(16):1958–1965
31. de Lemos JA, Drazner MH, Omland T, Ayers CR, Khera A, Rohatgi A, Hashim I, Berry JD, Das SR, Morrow DA (2010) Association of troponin T detected with a highly sensitive assay and cardiac structure and mortality risk in the general population. Jama 304(22):2503–2512
32. Mayilo S, Kloster MA, Wunderlich M, Lutich A, Klar TA, Nichtl A, Kürzinger K, Stefani FD, Feldmann J (2009) Long-range fluorescence quenching by gold nanoparticles in a sandwich immunoassay for cardiac troponin T. Nano Lett 9(12):4558–4563
33. Omland T, de Lemos JA, Sabatine MS, Christophi CA, Rice MM, Jablonski KA, Tjora S, Domanski MJ, Gersh BJ, Rouleau JL (2009) A sensitive cardiac troponin T assay in stable coronary artery disease. N Engl J Med 361(26):2538–2547
34. Reichlin T, Hochholzer W, Bassetti S, Steuer S, Stelzig C, Hartwiger S, Biedert S, Schaub N, Buerge C, Potocki M (2009) Early diagnosis of myocardial infarction with sensitive cardiac troponin assays. N Engl J Med 361(9):858–867
35. Mattos A, Freitas T, Silva V, Dutra R (2012) A dual quartz crystal microbalance for human cardiac troponin T in real time detection. Sensors Actuators B Chem 161(1):439–446
36. Silva BV, Cavalcanti IT, Silva MM, Dutra RF (2013) A carbon nanotube screen-printed electrode for label-free detection of the human cardiac troponin T. Talanta 117:431–437
37. de Ávila BEF, Escamilla-Gómez V, Campuzano S, Pedrero M, Pingarrón JM (2013) Disposable electrochemical magnetoimmunosensor for the determination of troponin T cardiac marker. Electroanalysis 25(1):51–58
38. Zanato N, Talamini L, Zapp E, Brondani D, Vieira IC (2017) Label-free electrochemical Immunosensor for cardiac troponin T based on exfoliated graphite Nanoplatelets decorated with gold nanoparticles. Electroanalysis 29(7):1820–1827
39. Barrett TW, Shanmugam NR, Selvam AP, Kazmierczak SC, Prasad S (2015) Novel Nanomonitor ultra-sensitive detection of troponin T. Clin Chim Acta 442:96–101
40. Brondani D, Piovesan JV, Westphal E, Gallardo H, Dutra RAF, Spinelli A, Vieira IC (2014) A label-free electrochemical immunosensor based on an ionic organic molecule and chitosan-stabilized gold nanoparticles for the detection of cardiac troponin T. Analyst 139(20):5200–5208
41. Gomes-Filho S, Dias A, Silva M, Silva B, Dutra R (2013) A carbon nanotube-based electrochemical immunosensor for cardiac troponin T. Microchem J 109:10–15
42. Hsueh H-T, Lin C-T (2016) An incremental double-layer capacitance of a planar nano gap and its application in cardiac-troponin T detection. Biosens Bioelectron 79:636–643
43. Jacobs M, Panneer Selvam A, Craven JE, Prasad S (2014) Antibody-conjugated gold nanoparticle-based immunosensor for ultra-sensitive detection of troponin-T. J Lab Autom 19(6):546–554
44. Mattos AB, Freitas TA, Kubota LT, Dutra RF (2013) An o-aminobenzoic acid film-based immunoelectrode for detection of the cardiac troponin T in human serum. Biochem Eng J 71:97–104
45. Munje RD, Jacobs M, Muthukumar S, Quadri B, Shanmugam NR, Prasad S (2015) A novel approach for electrical tuning of nano-textured zinc oxide surfaces for ultra-sensitive troponin-T detection. Anal Methods 7(24):10136–10144
46. Silva BV, Cavalcanti IT, Mattos AB, Moura P, Maria Del Pilar TS, Dutra RF (2010) Disposable immunosensor for human cardiac troponin T based on streptavidin-microsphere modified screen-printed electrode. Biosens Bioelectron 26(3):1062–1067
47. Zapp E, da Silva PS, Westphal E, Gallardo H, Spinelli A, Vieira IC (2014) Troponin T immunosensor based on liquid crystal and silsesquioxane-supported gold nanoparticles. Bioconjug Chem 25(9):1638–1643
48. Pawula M, Altintas Z, Tothill IE (2016) SPR detection of cardiac troponin T for acute myocardial infarction. Talanta 146:823–830
49. Dutra RF, Mendes RK, da Silva VL, Kubota LT (2007) Surface plasmon resonance immunosensor for human cardiac troponin T based on self-assembled monolayer. J Pharm Biomed Anal 43(5): 1744–1750
50. Liu JT, Chen CJ, Ikoma T, Yoshioka T, Cross JS, Chang S-J, Tsai J-Z, Tanaka J (2011) Surface plasmon resonance biosensor with high anti-fouling ability for the detection of cardiac marker troponin T. Anal Chim Acta 703(1):80–86
51. Ashaduzzaman M, Deshpande SR, Murugan NA, Mishra YK, Turner AP, Tiwari A (2017) On/off-switchable LSPR nano-immunoassay for troponin-T. Sci Rep 7
52. Yeom S-H, Kang B-H, Kim K-J, Yuan H, Kim O-G, Han M-E, Kwon D-H, Kang S-W Nanoporous aluminum anodic oxide-based optical biosensor for real-time detection of Troponin T. In: Sensors, 2011 IEEE, 2011. IEEE, pp 288–291
53. Zhang J, Kruss S, Hilmer AJ, Shimizu S, Schmois Z, De La Cruz F, Barone PW, Reuel NF, Heller DA, Strano MS (2014) A rapid, direct, quantitative, and label-free detector of cardiac biomarker troponin T using near-infrared fluorescent single-walled carbon nanotube sensors. Adv Healthc Mater 3(3):412–423
54. Moreira FT, Dutra RA, Noronha JP, Cunha AL, Sales MGF (2011) Artificial antibodies for troponin T by its imprinting on the surface of multiwalled carbon nanotubes: its use as sensory surfaces. Biosens Bioelectron 28(1):243–250
55. Zhang G-J, Luo ZHH, Huang MJ, Kang TG, Ji H (2011) An integrated chip for rapid, sensitive, and multiplexed detection of cardiac biomarkers from fingerprick blood. Biosens Bioelectron 28(1):459–463
56. Chua JH, Chee R-E, Agarwal A, Wong SM, Zhang G-J (2009) Label-free electrical detection of cardiac biomarker with complementary metal-oxide semiconductor-compatible silicon nanowire sensor arrays. Anal Chem 81(15):6266–6271
57. PatilM UF, Kormos R, Kumta PN (2018) Platinum aptasensor wire arrays for cardiac biomarker detection. Materials Today Communications 15:55–60
58. Miller J (1993) Statistics for analytical chemistry. Prentice Hall